# CSRR Based Sensors for Relative Permittivity Measurement With Improved and Uniform Sensitivity Throughout [0.9-10.9] GHz Band

Salem A. Alotaibi, *Student Member, IEEE*, Yepu Cui, *Student Member, IEEE*, and Manos M. Tentzeris, *Fellow, IEEE*

***Abstract*—This paper proposes miniaturized, lightweight and high sensitivity planar metamaterial based sensors for relative permittivity measurement within [0.9-10.9] GHz band. Each proposed sensor is designed using a thin-substrate microstrip line loaded with a single complementary split ring resonator (CSRR). The loaded resonator is excited using maximum electric/magnetic (cross polarization) excitation to maximize the sensors' sensitivity. Each proposed sensor operates at different frequency range within [0.9-10.9] GHz band based on the size of the loaded resonator. Compared to similar state-of-the-art sensors, the proposed ones are at least 30% more sensitive. The minimum transmission frequency shifts (50)% as the sample's relative permittivity changes from 1 to 10. The paper proposes a condition of sensitivity uniformity to maintain a uniform sensitivity over the specified band irrespective of the resonator size. Utilizing the proposed condition, the sensitivity of all sensors remains uniform throughout [0.9-10.9] GHz band for all dielectric samples with relative permittivity between 1 and 10. This vital feature allows the practical realization of resonant probes with less computational operations and consistent measurements over a wide dynamic range of the sensing-related frequency. Experimental measurements are in good agreement with the numerical findings. The paper includes a comprehensive sensitivity analysis which investigates the effect of resonator's excitation scheme, resonator's order (i.e. single or double CSRR) and substrate thickness on the sensitivity of CSRR based sensors. The proposed sensing platforms are recommended for the development of highly sensitive, consistent and reliable planar sensors such as microfluidics, displacement, nondestructive and biomedical sensors.**

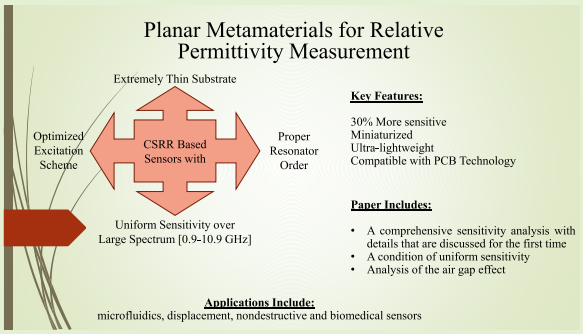


***Index Terms*—Material characterization, complementary split ring resonator (CSRR), planar metamaterials.**

## I. Introduction

ELECTROMAGNETIC wave propagation and scattering are controlled by materials configuration, electrical sizes, permittivity, and permeability. Precise identification of these parameters leads to accurate modeling and design of electromagnetic systems. Permittivity and permeability are, in general, functions of the interfering wave's frequency. However, permittivity has a stronger frequency dependence within RF and microwave frequency bands compared to permeability. Moreover, most dielectrics have poor magnetization properties within the same bands. Thus, the estimation of material's permittivity is more significant than permeability for the design of most electromagnetic systems.

Manuscript received August 17, 2019; revised September 27, 2019; accepted October 18, 2019. Date of publication November 4, 2019; date of current version April 3, 2020. The associate editor coordinating the review of this article and approving it for publication was Dr. Kagan Topalli. *(Corresponding author: Salem A. Alotaibi.)*

The authors are with the School of Electrical and Computer Engineering, Georgia Institute of Technology, Atlanta, GA 30332 USA (e-mail: otaisa1d@gatech.edu; otaisa1d@aramco.com).

Digital Object Identifier 10.1109/JSEN.2019.2951172

Several techniques have been utilized to estimate the electromagnetic properties of a material [1]–[18]. Material characterization using planar metamaterial transmission line is one of the emerging techniques. This technique depends on the direct interaction between the material under test (MUT) and the transmission line's evanescent field which results in high measurement accuracy and excellent imaging capability [19]–[21]. A planar metamaterial is composed of conventional transmission line loaded with a meta-resonator such as split ring resonator (SRR) or complementary split ring resonator (CSRR). Proper selection of the hosting transmission line as well as the resonating structure is an essential factor that controls the performance of the designed planar metamaterial (i.e. designed sensor).

Planar metamaterial was introduced for relative permittivity measurement in [12]. This paper utilized a microstrip line loaded with CSRR for characterization of homogenous dielectric samples. It should be noted that the measurement of a permittivity within a specific sensing zone can be utilized to identify a material of interest when a homogenous material occupies the whole sensing zone, and/or utilized

to measure a physical quantity of interest associated with a permittivity variation within a specified sensing zone. Numerous researchers have proposed different topologies of planar metamaterial for permittivity measurement [13]–[18] as well as other sensing applications with a narrower scope such as fluidic sensing [22]–[26], object's displacement and velocity [27]–[31], crack sensing [32]–[35], and organic tissues analysis [36].

The sensitivity of various sensors can be compared using the relation between the minimum transmission frequency and the MUT's relative permittivity. Previously proposed sensors had different operational bands and minimum transmission frequencies. It is expected that a sensor with a high free space minimum transmission frequency to have a higher shift magnitude (i.e. shift measured in GHz) compared to a sensor with a lower one when they are loaded with identical MUTs. Thus, to have a consistent sensitivity comparison irrespective of shift magnitude (i.e. irrespective of the resonator's size), it is recommended to compare the percentage of the minimum transmission frequency shift rather than the magnitude of minimum transmission frequency shift.

MUT's relative permittivity range is another crucial factor for consistent comparison. The MUT's equivalent capacitance is inversely proportional to the minimum transmission frequency shift increment. Consequently, as the permittivity of the loaded MUT's increases, the increment in the magnitude and percentage of the minimum transmission frequency shift with respect to free space minimum transmission frequency decreases. For large permittivity, the corresponding increment starts to be negligible. For this reason, the sensitivity of a permittivity sensor with a free space minimum transmission frequency less than 10 GHz could be evaluated efficiently using MUTs with a variable relative permittivity between 1 and 10. Table I shows a sensitivity comparison based on the percentage of the minimum transmission frequency shifts as the MUT's relative permittivity changes from 1 to 10 for previous studies that used CSRR based sensors for permittivity measurements. The basic configuration of the compared sensors is similar where a coaxial line is used to feed a microstrip transmission line (MTL) loaded with a CSRR. These studies used the same alignment of single or double CSRR with respect to the MTL strip (i.e. the resonator's slit is oriented perpendicularly to the MTL strip). The used orientation ensures resonance excitation with pure electric excitation through the time-varying electric field between the MTL strip and the ground plane.

The reported studies did not investigate the effect of different excitation schemes, resonator's order (i.e. single or double) and substrate thickness on the sensitivity of the proposed sensors. They also did not examine the performance of the proposed sensors at different frequency bands to outline the necessary condition to maintain a uniform sensitivity over various frequency bands.

This paper proposes thin substrate sensors with an improved and uniform sensitivity over a broad spectrum using single CSRR excited with cross polarization excitation. The paper is organized as follows. Section II details the operation theory of the proposed sensors. Section III provides a comprehensive sensitivity analysis where the effect of the excitation scheme, resonator's order, and substrate thickness on the sensors' sensitivity are thoroughly investigated. This section also presents a condition of sensitivity uniformity with the required proof of concept. Section IV summarizes the sensors' design and outlines the measurement procedure. The experimental results are presented in section V. Air gap effect is numerically studied in section VI. The paper is concluded with a summary, improvement opportunities and potential applications.

TABLE I
COMPARISON WITH SIMILAR STATE OF THE ART SENSORS

| Ref. | Freq. Band (GHz) | Resonator | Freq. Shift |
|---|---|---|---|
| [12] | 0.8-1.3 | Double CSRR | 38 % |
| [13] | 1.8-2.8 | Double CSRR | 36% |
| [14] | 1.08-1.63 | Single CSRR | 34% |
| [14] | 2.16-3.33 | Single CSRR | 35 % |
| [15] | 1.75-2.7 | Double CSRR | 35% |
| [16] | 5.23-8.45 | Double CSRR | 38% |
| This Work | 0.90-10.90 | Single CSRR | 50% |

## II. OPERATION THEORY

Each proposed sensor is designed using a microwave planar transmission line (MTL) that is loaded with a passive resonator (CSRR). Every transmission line has its unique electric and magnetic field profiles within and around its spatial extent. The resonance of a passive resonator can be optimally excited using optimum alignment between the resonator and interacted electric and/or magnetic fields. Therefore, it is necessary for a sensor designer to understand transmission lines' propagating modes and fields' profiles as well as resonator excitation requirements to be able to select a transmission line that better fits the resonator's optimum excitation scheme. The following subsections provide a smooth background that rationalizes the utilization of microstrip line loaded with scalable CSRR in this paper to realize high sensitivity relative permittivity sensors.

### A. Defected Ground Structure and Substrate Inclusion

MTL and Coplanar waveguide (CPW) are two of the most popular planar transmission lines. Both lines are used primarily for low power signal transmission. However, their function could be altered by changing their configurations or by adding other passive or active elements to realize numerous microwave circuit components such as resonator-based sensors, filters and antennas. This paper proposes sensors that are designed using planar transmission line loaded with scalable resonators. One way to realize such device, is to load the transmission line with either a conductive substrate inclusion or a ground plane defect.

Defected ground structure (DGS) and conductive substrate inclusions have been extensively utilized for various sensing and filtering applications [12]–[18], [22]–[38]. Ground defects and substrate inclusions are coupled to the quasi-TEM mode of the MTL or CPW. TEM mode is intense within a limited volume of the substrate of these transmission

lines [39]. This limitation restricts the designer's choice of ground defect/substrate inclusion position within the hosting transmission line for proper coupling (excitation) purposes. Ground defect and substrate inclusion form mismatched loads, therefore they enforce new boundary conditions that change the profile of the original fields and induced currents within the hosting transmission line, which consequently causes a wave reflection and possibly a resonance at specific frequency band. For this reason, these two structures are considered as resonators.

Resonance occurs when a system stores an oscillating and balanced electric and magnetic energy. When a microwave circuit resonates, electric and magnetic energy oscillates between each other. The resonance frequency of the microwave resonator changes when the distribution of the electromagnetic fields within the resonator vicinity perturbs. This is due to the variation of the overall system's effective permittivity and permeability. The word system is referred to the resonator and the surrounding environment which includes interacted electromagnetic fields and/or electrically close objects. Accordingly, when MUT brought into direct contact or close proximity to a resonating structure or when it interferes with the guided waves within a resonating structure, it perturbs its electromagnetic fields distribution and consequently its resonance frequency changes. The change in the resonance frequency and the MUT properties can be related to each other using cavity perturbation relation in (1) [12].

$$\frac{\Delta f_r}{f_r} = \frac{\int_v \left(\Delta\varepsilon \mathbf{E}_1 \cdot \mathbf{E_0} + \Delta\mu \mathbf{H}_1 \cdot \mathbf{H_0}\right) \boldsymbol{dv}}{\int_v \left(\varepsilon_0 |\mathrm{E}_0|^2 + \mu_0 |\mathrm{H}_0|^2\right) \boldsymbol{dv}} \tag{1}$$

where $\Delta f_r$ is the shift in the resonance frequency $f_r$, $\Delta\varepsilon$ and $\Delta\mu$ are the change in the permittivity and permeability, respectively. $\varepsilon_0$ and $\mu_0$ are the free space permittivity and free space permeability, respectively. $\mathbf{E_0}$ and $\mathbf{H_0}$ are the original fields. $\mathbf{E}_1$ and $\mathbf{H}_1$ are the fields with perturbation. $\boldsymbol{v}$ is the perturbed volume.

For extremely low power resonator with negligible variation in the magnitude of the electric and magnetic fields before and after the resonance, the relation can be simplified to (2)

$$\frac{\Delta f_r}{f_r} = \frac{\int_v \left(\Delta\varepsilon |\mathrm{E}_0|^2 + \Delta\mu |\mathrm{H}_0|^2\right) \boldsymbol{dv}}{\int_v \left(\varepsilon_0 |\mathrm{E}_0|^2 + \mu_0 |\mathrm{H}_0|^2\right) \boldsymbol{dv}} \tag{2}$$

For sensing applications, the design and parameter selections of the planar transmission line as well as the defect/inclusion should be optimized to maximize the resonance strength and to optimally confine the resonating electrical (magnetic) fields within permittivity (permeability) sensing area. Moreover, the resonator's selection should consider the available excitation power by the feeding network. For example, it is expected that numerous sensing spots will be utilized for the emerging internet of things (IoT) applications where each point will have very low power [40]. Thus, utilization of electrically small resonators with almost zero power is a preferred choice for such applications.

### B. Resonator Type

Split ring resonator (SRR) and its complement (CSRR) are electrically small structures with circular current paths which in turns develop tightly spaced inductance(s) and capacitance(s) at resonance. Such structures reduce the length of the current path required by conventional transmission line resonators which allow the realization of miniaturized resonator-based devices [12]. Fig.1 shows a layout of double square SRR and CSRR. Single SRR or CSRR can be obtained by simply removing the inner or outer ring of the double counterpart. In principle, SRR and its complement can be magnetically and/or electrically excited. However, the normal time-varying magnetic (electric) field is considered as the dominant SRR (CSRR) excitation. For this reason, to ensure proper excitation of these resonators when loaded to a transmission line, SRR is placed as a substrate conductive inclusion in the bottom of a CPW substrate centered at the narrow gap between one of the ground strips and the central signal strip. On the other hand, CSRR is placed as a ground defect in the MTL ground plane normal to the MTL strip [41]. This excitation schemes forces, conduction current circulation within the SRR circumference and magnetic current (fictitious) circulation within the CSRR circumference. It should be noted that a CSRR loaded to a transmission line is not a perfect complement of its counterpart due to the presence of the dielectric substrate and finite ground plane [41]. However, the overall expected response of the exact CSRR is slightly affected by these two factors especially for a thin substrate with low permittivity.

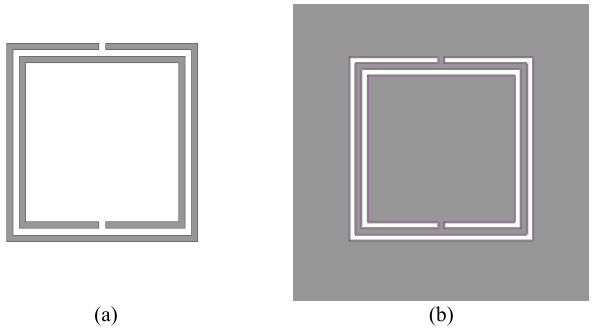


Fig. 1. The layout of double (a) SRR (b) CSRR. Gray color designates conductive material.

For electrically small resonators, the size of the sensing zone determines which resonator to be utilized as the captured energy is relatively low for both resonators. At resonance, CPW loaded with SRR concentrates the resonating electric field within its slit while MTL loaded with CSRR has larger concentration area within its circumference. Therefore, each proposed sensor in this paper is designed using MTL loaded with a CSRR.

## III. Sensitivity Analysis

A comprehensive sensitivity study was conducted to investigate the effect of various excitation schemes, CSRR's order (i.e. single or double) and substrate thickness on the sensitivity of a CSRR based sensor. Throughout this paper the considered cases were numerically studied using full-wave numerical simulation package ANSYS HFSS. The simulation setup consists of a planar sensor loaded with a variable permittivity MUT positioned underneath the MTL ground plane in direct contact

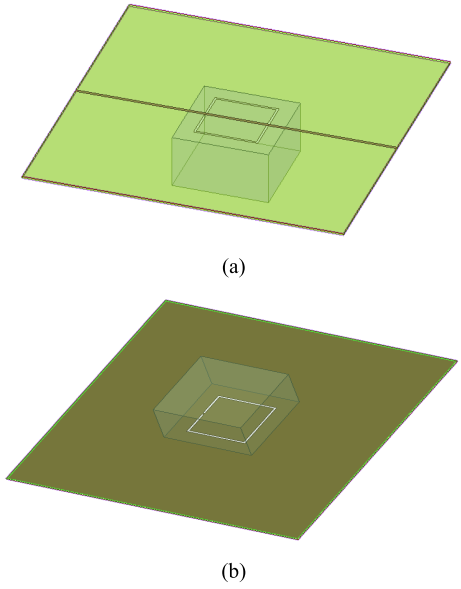

Fig. 2. (a) Top (b) bottom view of the general sensors' setup. The etched resonator in this figure is a single CSRR with cross polarization excitation. The MUT appears as a semi-transparent cube attached to the ground plane.

with the etched CSRR. For all cases, the used CSRR is a square CSRR with a path width of 0.2mm. The split length as well as the separation between inner and outer rings for double CSRR are also 0.2mm for all cases. The used MUT is a rectangular dielectric cube with a 5-mm height. The width and length of the MUT are identical and assumed to be two times higher than the side length of the square CSRR. The planar center of the CSRR and the interfaced MUT's surface coincides. Except for the air gap study at the end of this paper, the MUT is assumed to be in direct contact with the etched CSRR. Fig.2(a) and Fig.2(b) show the general sensors' setup. For each studied case, the general structure was changed based on the case-specific excitation scheme, CSRR's order (single or double), substrate thickness and CSRR side length (CSRR's size).

Minimum transmission frequency was used to define the sensitivity of the proposed sensors. The minimum transmission frequency of MTL loaded with a CSRR is given by (3) [42]. The change in the minimum transmission frequency was calculated based on (4). The sensitivity of a CSRR based sensor at each studied case was calculated based on the percentage change in the minimum transmission frequency as given by (5).

$$f_{MUT0}^{tmin} = \frac{1}{2\pi\sqrt{L_{CSRR}(C_{CSRR}+C_{MUT})}} \tag{3}$$

$$\Delta f^{tmin} = f_{MUT0}^{tmin} - f_{free}^{tmin} \tag{4}$$

$$\Delta f^{tmin}\% = \left(\frac{f_{MUT0}^{tmin} - f_{free}^{tmin}}{f_{free}^{tmin}}\right) \times 100 \tag{5}$$

where $f_{MUT0}^{tmin}$ is the minimum transmission frequency at the presence of MUT with a 0-mm air gap. $L_{CSRR}$ and $C_{CSRR}$ are the equivalent inductance and capacitance of the loaded CSRR, respectively. $C_{MUT}$ is the equivalent capacitance of the loaded MUT. $f_{free}^{tmin}$ is the free space minimum transmission frequency (i.e. $f_{free}^{tmin} = f_{MUT0}^{tmin}$ with $C_{MUT} = 0$) $\Delta f^{tmin}$ is the change in the minimum transmission frequency in GHz. $\Delta f^{tmin}\%$ is the percentage change in the minimum transmission frequency.

### A. CSRR Excitation: Pure Electric Vs. Electric/Magnetic

CSRR loaded to a waveguide can be excited using electric and/or magnetic excitations [41]. However, CSRR loaded to MTL has limited excitation choices as pure magnetic excitation is not realizable. Excitation's strength and type can be controlled by rotating the CSRR's magnetic wall (i.e. line of symmetry for a square CSRR) with respect to the axis of the MTL conducting strip. CSRR is excited using electric excitation when its magnetic wall is orthogonal with respect to the MTL conducting strip. On the other hand, CSRR is excited using electric/magnetic excitation when its magnetic wall is not orthogonal with respect to the MTL strip. As a special case, when the magnetic wall of the loaded CSRR is parallel with respect to the MTL conducting strip, then the CSRR will be excited with maximum electric/magnetic excitation. This type of excitation is also called cross polarization excitation [43]. In this paper we will refer to electric excitation as pure electric excitation to further stress that the magnetic field effect in this type of excitation is negligible.

Four cases were simulated to extract the relative permittivity of the MUT using a 6-mm square CSRR with identical MUTs. The aim of these cases is to study the influence of the CSRR's excitation scheme on the sensors' sensitivity. For each case, the utilized MTL has a 0.125-mm substrate thickness with a dielectric constant of 2.9 and a strip width of 0.267mm. The relative permittivity of the MUT was varied from 1 to 10 with a 0.25-step. A single CSRR was used for the first two cases with pure electric excitation in one case as shown in Fig.3(a) and a maximum electric/magnetic (cross polarization) excitation in the other one as shown in Fig.3(b). A double CSRR was used for the third and fourth cases with pure electric excitation in one case as shown in Fig.3(c) and maximum electric/magnetic (cross polarization) excitation in the other one as shown in Fig.3(d).

The sensitivity of the four simulated sensors was compared based on the change in the minimum transmission frequency as defined by (5). Fig.4 shows the results of the first two cases while Fig.5 shows the results of the third and fourth cases. The obtained results show higher sensitivity for the sensors with maximum electric/magnetic (cross polarization) excitation compared to the ones with pure electric excitation for either single or double CSRR.

To further investigate the influential factor that causes this superiority, a fifth simulation case was added. In this case a single 6-mm square CSRR based sensor was used with seven excitation schemes ranging from pure electric to maximum electric/magnetic (cross polarization) excitation. The seven schemes were realized by rotating the CSRR's magnetic wall from its reference position (0°) (i.e. Fig.3(a)) which corresponds to pure electric excitation toward (90°) (i.e. Fig.3(b)) which corresponds to maximum electric/magnetic

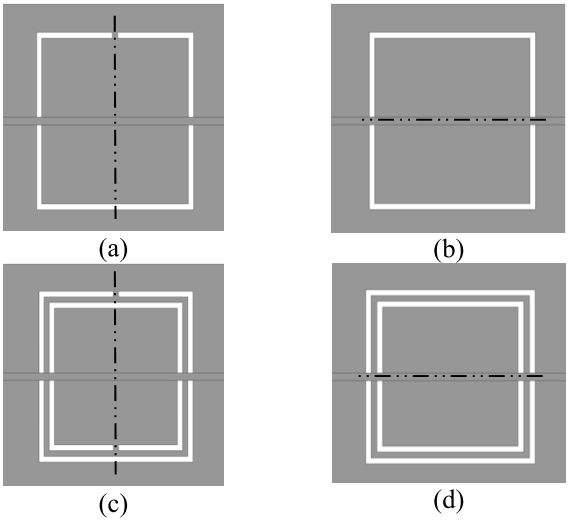


Fig. 3. Top view of MTL loaded with square (a) single CSRR with pure electric excitation (b) single CSRR with cross polarization excitation (c) double CSRR with pure electric excitation (d) double CSRR with cross polarization excitation. The dashed lines show the magnetic wall of the loaded CSRR.

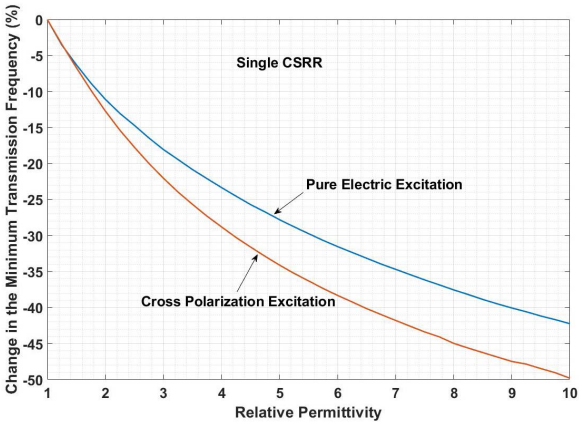


Fig. 4. Change in the minimum transmission frequency versus MUT's relative permittivity for single CSRR with pure electric (blue) and cross polarization (red) excitation. (Simulation results).

(cross polarization) excitation using a 15-degree step. It should be noted that as the rotation angle increases from 0° to 90°, the influence of the exciting magnetic field increases [43].

Fig.6 shows the minimum transmission frequency for the seven excitation schemes while Fig.7 shows the variation of the minimum transmission frequency for the same cases. These figures show almost identical minimum transmission frequency for the sensors with CSRRs at 0° (pure electric excitation), 15° and 30° (both have different levels of electric/magnetic excitation). This indicates that the exciting magnetic field or more specifically its induced currents do not have a noticeable contribution to the equivalent inductance and capacitance of the CSRR and consequently do not alter its minimum transmission frequency. However, as the excitation gradually moves toward a higher electric/magnetic excitation scheme, the sensors' sensitivity starts to vary. From 30° angle upward, the exciting magnetic field begins to have a noticeable

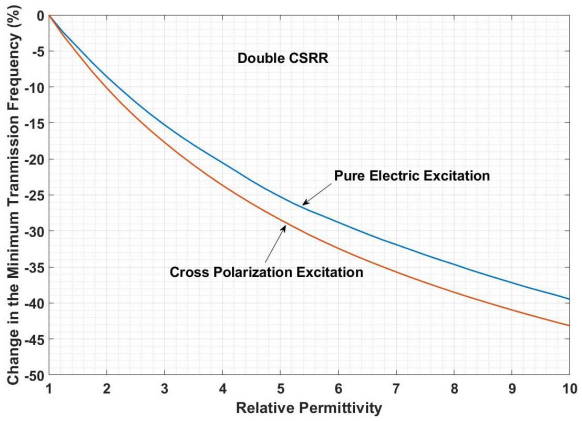


Fig. 5. Change in the minimum transmission frequency versus MUT's relative permittivity for double CSRR with pure electric (blue) and cross polarization (red) excitation. (Simulation results).

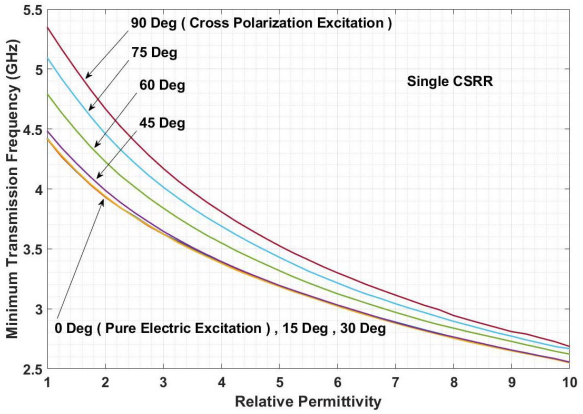


Fig. 6. Minimum transmission frequency versus MUT's relative permittivity for single CSRR with seven excitations ranging from pure electric (0°) to cross polarization (90°) excitation using a 15- degree step. (Simulation results).

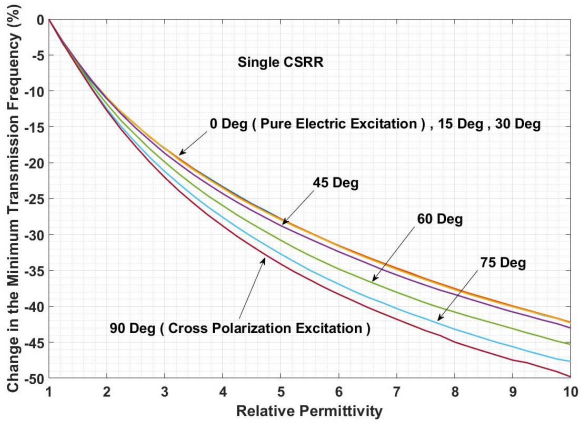


Fig. 7. Change in the minimum transmission frequency versus MUT's relative permittivity for single CSRR with seven excitations ranging from pure electric (0°) to cross polarization (90°) excitation using a 15- degree step. (Simulation results).

influence which is revealed by the gradual increase in the free space minimum transmission frequency as shown in Fig.6 as well as the gradual rise in the sensors' sensitivity as shown in

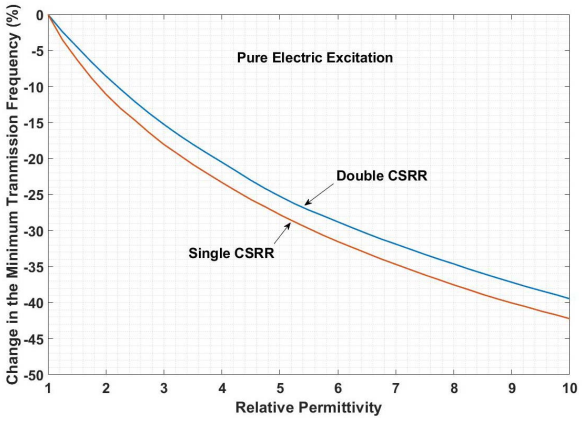


Fig. 8. Change in the minimum transmission frequency versus MUT's relative permittivity for single (red) and double (blue) CSRR with pure electric excitation. (Simulation results).

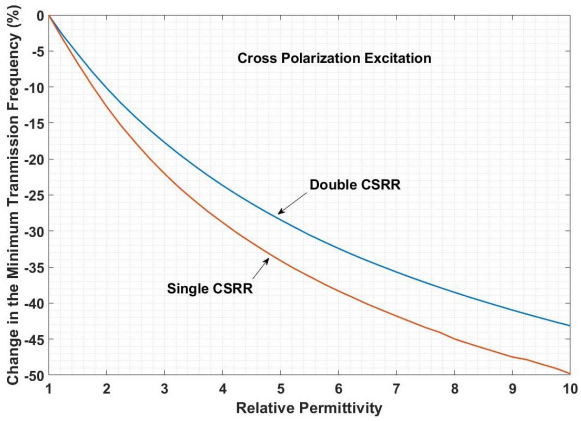


Fig. 9. Change in the minimum transmission frequency versus MUT's relative permittivity for single (red) and double (blue) CSRR with cross polarization excitation. (Simulation results).

Fig.7. Based on (3), the gradual increase in the free space minimum transmission frequency is a sign of a reduction in the combined CSRR equivalent reactive elements term ($L_{CSRR}\times C_{CSRR}$). Such reduction increases the dependence of the minimum transmission frequency on the ($L_{CSRR}\times C_{MUT}$) term or more specifically on the loaded MUT permittivity that is modelled by $C_{MUT}$. This justifies the superiority of CSRR based sensors with maximum electric/magnetic (cross polarization) excitation scheme with respect to other excitation schemes.

### B. Single Vs. Double CSRR

The reported studies in the introduction utilized either single or double CSRR for materials characterization. To the best knowledge of the authors, the optimum choice of either single or double CSRR for material characterization using MTL based sensors has not been investigated before. Here we are performing a systematic sensitivity comparison between two sensors with identical substrate and MUTs. The first one uses a single 6-mm square CSRR while the other one uses a double 6-mm square CSRR. Four cases were simulated to extract the relative permittivity of loaded MUTs using the specified sensors. In each case the relative permittivity of the MUTs were varied from 1 to 10 with a 0.25-step. In the first two cases a single and a double CSRR with pure electric excitation were used. The third and fourth cases have a single and a double CSRR with maximum electric/magnetic (cross polarization) excitation. Fig.8 shows the results of the first two cases while Fig.9 shows the results of the third and fourth cases. The results confirm the superiority of the MTL sensors with single CSRR over the ones with double CSRR for relative permittivity measurements. This superiority is irrespective of the used excitation scheme, as the single CSRR sensors were more sensitive in both excitation schemes. The obtained results are expected as double CSRR has two concentric rings with a very small separation between the inner and the outer rings. This configuration increases the equivalent capacitance of the resonator, which consequently reduces the dependence of the sensor's minimum transmission frequency on the MUT's equivalent capacitance.

### C. Substrate Thickness Effect

The dielectric substrate is a medium through which a substantial portion of the guided EM waves propagates in electrically thick MTL. When a given structure resonates, the resonating electric field polarizes the surrounding dielectrics. Each homogenous polarized dielectric can be represented by an equivalent capacitance. Thus, for a given MTL that is loaded with a CSRR, the resonating electric field polarizes a portion of the MTL substrate and a portion of the loaded MUT if any. $C_{CSRR}$ and $C_{MUT}$ depend on the polarized portion of the substrate and the polarized portion of the loaded MUT, respectively. Reducing the polarized portion of the MUT, decreases the dependence of the minimum transmission frequency on $C_{MUT}$ and decreases the sensor's sensitivity. For this reason, the used MUTs in this paper have a 5-mm height to ensure efficient interaction with the resonating electric field. Furthermore, reducing the polarized portion of the substrate increases the polarized portion of the loaded MUT which consequently increases the dependence of the minimum transmission frequency on $C_{MUT}$ and increases the sensor's sensitivity. Reducing the polarized portion of the substrate can be achieved by reducing the portion of the substrate that falls under the influence of the resonating electric field. This reduction can be realized by reducing the thickness of the substrate.

Eight cases were considered where we studied the sensitivity of various CSRR based sensors with different substrate thicknesses. In each case a single 6-mm square CSRR with cross polarization excitation was utilized as a sensor's resonator. Eight different sensors with eight different substrate thicknesses were considered. The dielectric constant of the used substrates is 2.9. Each sensor has different MTL strip width to match its impedance to the feeding network impedance (i.e.50-ohm). For each case, the relative permittivity of the loaded MUT was varied from 1 to 10 with a 0.25-step. The results of the considered cases are shown in Fig.10

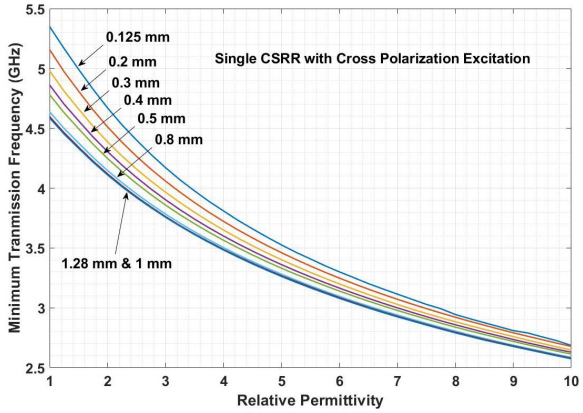


Fig. 10. Minimum transmission frequency versus MUT's relative permittivity for CSRR based sensors with different substrate thicknesses. (Simulation results).

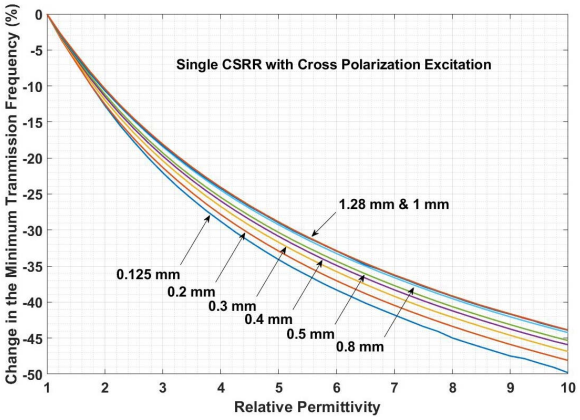


Fig. 11. Change in the minimum transmission frequency versus MUT's relative permittivity for CSRR based sensors with different substrate thicknesses. (Simulation results).

and Fig.11. The utilized thicknesses are also shown in the figures. The obtained results show that the free space minimum transmission frequency is higher for CSRR based sensors with thinner substrates. As per (3), this indicates that the combined CSRR equivalent reactive elements term ($L_{CSRR} \times C_{CSRR}$) is smaller for thinner substrates which consequently increases the dependence of the minimum transmission frequency on the loaded MUT. Thus, the sensitivity of the sensor with the thinnest substrate used in these cases (i.e. 0.125mm) has the highest sensitivity as shown in Fig.11. It should also be noted that for relatively thicker substrates (i.e. 1mm and 1.28mm in these cases), the minimum transmission frequency and the sensor's sensitivity of a CSRR based sensor do not depend on the substrate thickness. This can be understood based on the discussed polarization mechanism in the previous paragraph. As the thickness of the substrate increases, the polarized substrate portion increases which increases $C_{CSRR}$. At a certain thickness, the substrate portion which is close to the CSRR will be completely polarized and the $C_{CSRR}$ will be fixed. Any increment in the substrate thickness will add additional substrate or additional dielectric layers which will not be under the influence of the resonating electric field and consequently will not affect the minimum transmission frequency and the sensor's sensitivity as it will not change the equivalent capacitance of the CSRR.

### D. Sensitivity Uniformity

Relative permittivity is a frequency dependent parameter. A single sensor that operates within a specific band of frequency is required to extract material's relative permittivity within a specified band. However, if the characterization is going to be conducted over different frequency bands, different sensors are needed where each sensor has its own frequency range of operation and its own sensitivity. Therefore, if the sensitivity of the utilized sensors is different, the obtained relative permittivities will not be consistent. To overcome this problem, a general condition of sensitivity uniformity is proposed in this paper for CSRR based sensors that are utilized for relative permittivity measurement. For completeness, another general condition of sensitivity uniformity is also proposed for relative permeability measurement. The proposed conditions are presented in the paper's Appendix.

The minimum transmission frequency of MTL based resonator can be varied by varying the substrate's thickness, its dielectric constant or resonator's design parameters. Changing a substrate thickness and/or its dielectric constant may require an associated change of the MTL strip width to match it to the feeding network impedance. Uncontrolled variation of all or some of these three parameters may result in an unpleasant disorder of wave confinement within the MTL substrate which drastically reduces the amount of the fields at the resonator vicinity and consequently reduces its sensitivity. It will also cause different sensitivity for different frequency bands due to the variation of wave confinements within the MTL substrate. Therefore, changing one or more of the resonator's parameters (i.e. the size of CSRR in this paper) would be a better option to vary the minimum transmission frequency which will consequently change the frequency band of operation. Sensitivity uniformity across a large spectrum could be achieved using the condition of sensitivity uniformity which is derived in the Appendix.

Sixteen cases were considered to study the sensitivity uniformity of a thin substrate MTL loaded with a single square CSRR and excited using cross polarization excitation. Each case, has a specific CSRR size, MUT size and frequency band of operation. To vary the frequency of operation, the size of the loaded CSRR was varied by varying its side length from 3mm to 18mm with a 1-mm step. To maintain a uniform sensitivity, the ratio between $C_{CSRR}$ and $C_{MUT}$ maintained constant (see Appendix). Thus, for each scaled CSRR, the width and length of the MUT assumed to be identical and to be two times higher than the side length of the scaled CSRR. For example, for a CSRR with a 3-mm side length the loaded MUT has a length and width of 6-mm. For each case, the relative permittivity of the loaded MUT was varied from 1 to 10 with a 0.25-step.

The minimum transmission frequency and corresponding sensitivity of the tested sensors are presented in Fig.12 and Fig.13, respectively. The presented results declare excellent sensitivity uniformity throughout [0.90-10.90] GHz band for each relative permittivity and each utilized sensor. As this

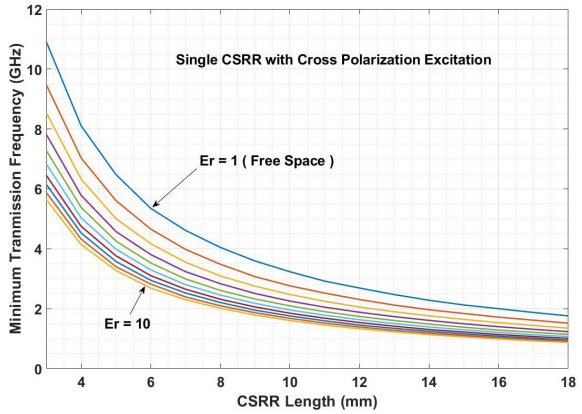


Fig. 12. Minimum transmission frequency versus CSRR side length for MUTs with relative permittivity ranging from Er = 1 to Er = 10. The curves are in sequence from top to bottom starting from Er = 1 (at the top) to Er = 10 (at the bottom). (Simulation results).

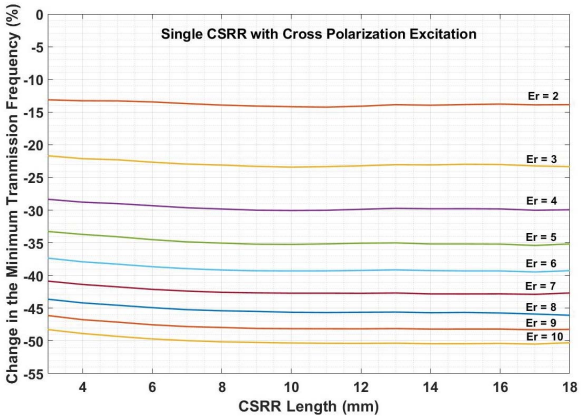


Fig. 13. Change in the minimum transmission frequency versus CSRR side length for MUTs with relative permittivity ranging from Er = 2 to Er = 10. The curves are in sequence from top to bottom starting from Er = 2 (at the top) to Er = 10 (at the bottom). (Simulation results).

band encompasses all used bands in the previously proposed sensors in [12]–[16], these results verify the superiority of the proposed sensors sensitivity over previously reported ones even within their bands.

Here is another advantage of the condition of sensitivity uniformity. Previous studies estimated MUT's permittivity using a single equation that relates MUT's permittivity to the measured magnitude of change in the minimum transmission frequency (i.e. eq.4) rather than the percentage of change (i.e. eq.5) [12]–[16]. Following such procedure for a multi-band sensor requires extraction of a unique equation for each frequency band. However, when the sensor's sensitivity is independent of the frequency band of operation, we can extract a single equation that can be utilized over a large spectrum by relating the MUT's permittivity to the measured change in the minimum transmission frequency ratio or percentage (i.e. eq.5) rather than frequency shift magnitude (i.e. measured in GHz as per eq.4). This is a vital feature especially when such sensors are utilized as sensing spots for massive sensors network applications such as IoT where networks' computational power are limited [40]. The relation between the free space minimum transmission frequency and the side length of the square CSRR is given in (6). A single relation that relates the MUT's relative permittivity to the change in the minimum transmission frequency for all considered sensors that operate at different frequency bands is given in (7).

$$f_{free}^{tmin} = 0.00058 \times Length_{CSRR}^{4} - 0.03 \times Length_{CSRR}^{3} + 0.57 \times Length_{CSRR}^{2} - 5 \times Length_{CSRR} + 19 \quad (6)$$

$$\varepsilon_{MUT0} = -6.7 \times 10^{-5} \times \left(\Delta f^{tmin}\%\right)^{3} - 0.0016 \times \left(\Delta f^{tmin}\%\right)^{2} - 0.096 \times \Delta f^{tmin}\% + 0.94 \quad (7)$$

where $f_{free}^{tmin}$ is the free space minimum transmission frequency in (GHz), $Length_{CSRR}$ is the CSRR side length in (mm), $\varepsilon_{MUT0}$ is the estimated MUT's relative permittivity and $\Delta f^{tmin}\%$ is the change in the minimum transmission frequency.

## IV. Sensors Design

This section summarizes the design of the proposed sensors. Each proposed sensing platform is composed of a 30-mm by 30-mm MTL loaded with a single square CSRR. The resonator line of symmetry coincides with the MTL strip projection on the ground plane as shown in Fig.2(b). This CSRR/MTL strip configuration ensure resonator's excitation with maximum electric/magnetic (cross polarization) excitation. The MTL is expected to be fed with a coaxial cable with a 50-ohm impedance. To match the MTL to the impedance of the feeding network, the conducting strip is designed with a 0.267 mm strip width. CSRR path width is 0.2 mm. CSRR split length is identical to its path width (i.e.0.2 mm). The used substrate has a 0.125 mm thickness with a dielectric constant of 2.9. The size of the loaded CSRR can be scaled to vary the minimum transmission frequency and the associated frequency band of operation as per Fig.12. In this study the side length of the square CSRR was scaled from 3mm to 18mm with a 1-mm step for performance verification. The corresponding frequency band of operation for MUT with relative permittivity ranging from 1 to 10 is [0.90 to 10.90] GHz. It should be noted that the proposed sensors' can also be utilized outside this range with larger CSRRs or with MUTs with higher relative permittivity. However, this range is the range through which the performance of the proposed sensors' was studied.

The following steps summarize the required procedure to measure MUT's relative permittivity using the proposed sensors:

1. Identify the band of operation based on the MUT intended application.
2. Select a CSRR side length $\left(Length_{CSRR}\right)$ that better fits the identified band of operation using Fig.12 and Fig.13.
3. Use the selected $\left(Length_{CSRR}\right)$ to calculate the free space minimum transmission frequency $(f_{free}^{tmin})$ using (6).
4. Fabricate the sensor using the selected $\left(Length_{CSRR}\right)$ and the detailed MTL specifications then measure its $(f_{free}^{tmin})$ experimentally and confirm that it matches the calculated one from step (3).

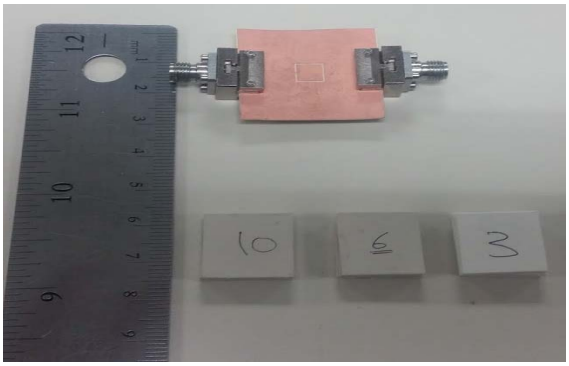

Fig. 14. Fabricated sensor and three MUTs fabricated using Roger substrates RO3003, RO3006 and RO3010.

5. Load the sensor with a MUT then measure the new minimum transmission frequency ($f^{tmin}_{MUT0}$).
6. Calculate the change in the minimum transmission frequency ($\Delta f^{tmin}\%$) by substituting the measured ($f^{tmin}_{free}$) and ($f^{tmin}_{MUT0}$) using (5).
7. Use (7) and the calculated ($\Delta f^{tmin}\%$) from step (6) to calculate MUT's relative permittivity ($\varepsilon_{MUT0}$).

## V. Experimental Measurements

To verify the performance of the proposed sensors experimentally, a prototype sensor was fabricated using a 30-mm by 30-mm low loss flexible substrate. The dielectric constant of the substrate is 2.9 with a 0.116 mm thickness. This substrate is slightly thinner than the used one in the previous sections (i.e. 0.125mm) however, such fabrication error is expected for thin substrates. A single square CSRR with a 6-mm side length was etched in the ground plane. The CSRR excited using cross polarization excitation. The path width as well as the split length is 0.2mm. The planar sensor is fed with a 50-ohm coaxial cable. The obtained free space minimum transmission frequency is 5.39 GHz. This frequency is almost in the middle of the sensors' free space minimum transmission frequencies. Hence, the selection of this sensor is an optimal choice for experimental verification. Three cubic MUTs were fabricated using Roger substrates RO3003, RO3006 and RO3010. The nominal relative permittivities of these substrates are 3, 6.15 and 10.2, respectively. Each MUT was constructed by vertically stacking four layers of corresponding copper free substrate. Each layer is a 15 mm by 15mm layer. Fig.14 shows the fabricated porotype and the constructed MUTs. Four measurements were obtained. The first one is the free space minimum transmission frequency. The other three are the minimum transmission frequencies of the RO3003, RO3006 and RO3010 MUTs. The MUTs minimum transmission frequencies were obtained by placing each MUT directly underneath the MTL with direct contact with the CSRR to interrupt its resonating fields. Fig.15 shows the obtained experimental measurements as well as the corresponding numerical results. The experimental and numerical results are in a good match. The simulation results presented in Fig.15 are extracted using a 0.116 mm substrate. The little mismatch is caused by the air gap between the MUTs layers which reduces their corresponding effective permittivity. Another source of error is

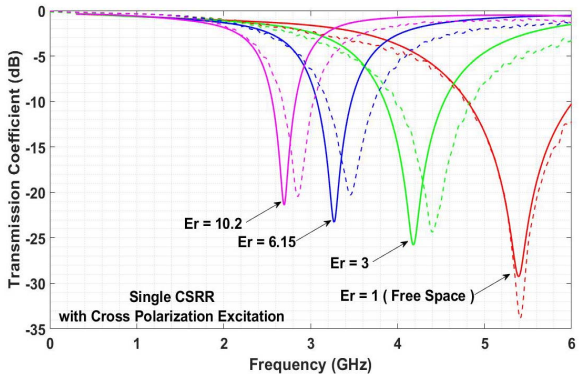


Fig. 15. Comparison between numerical (solid line) and experimental (dashed lines) results for the 6-mm CSRR based sensor. The red curve for Er = 1.The used MUTs have relative permittivities of Er = 3 (green), Er = 6.15 (blue) and Er = 10.2 (pink). (Simulation and measurement results).

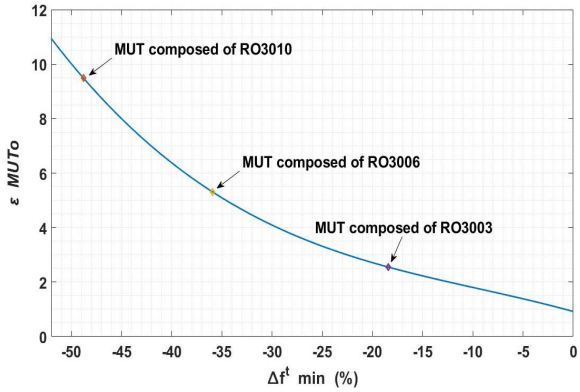


Fig. 16. Comparison between the results obtained by model (8) and the measurement results. (Simulation and measurement results).

the air gap layer between the CSRR footprint and the MUTs. This effect is discussed in the next section.

The relation between the MUT's relative permittivity and the change in the minimum transmission frequency based on the used substrate in this section (i.e. a substrate with a 0.116 mm thickness) is given by (8). The definitions of the used parameters in this equation are identical to the used ones in (7). Fig.16 shows a comparison between the results obtained by model (8) and the measurement results.

$$\varepsilon_{MUT0} = -7.35\times10^{-5}\times\left(\Delta f^{tmin}\%\right)^3 - 0.00207 \times\left(\Delta f^{tmin}\%\right)^2 - 0.10166\times\Delta f^{tmin}\% + 0.92 \quad (8)$$

## VI. Air Gap Effect

Previous numerical results assumed direct contact between the CSRR footprint and the loaded MUT. This setup ensures perfect coupling as the CSRR's resonating fields are in a sole interaction with the MUT at the sensing zone. However, in practice an air layer may exist between the two objects forming an air gap. Presence of an air gap alters the equivalent resonator's load capacitance which consequently introduces an error in the obtained measurements. The introduced error is directly proportional to the air layer's thickness and the MUT relative permittivity.

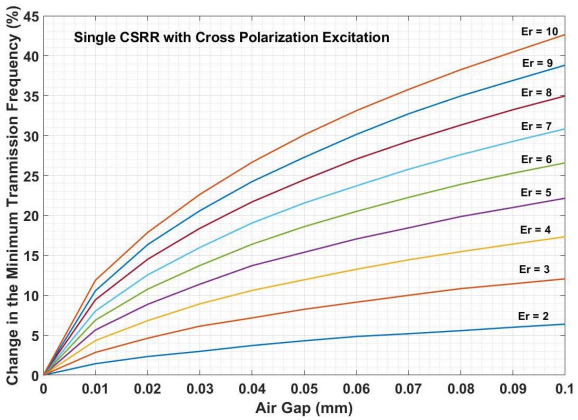


Fig. 17. Change in the minimum transmission frequency versus air layer thickness for MUTs with relative permittivity ranging from Er = 2 to Er = 10. The curves are in sequence from bottom to the top starting from Er = 2 (at the bottom) to Er = 10 (at the top). (Simulation results).

For a permittivity sensor's with a uniform air layer (i.e. air layer with a constant thickness all over the CSRR footprint), the air gap can be modeled with two equivalent capacitances in series with the MUT's equivalent capacitance [44]. As the thickness of the air gap increases its equivalent capacitance decreases consequently the resonator's load formed by the three series capacitances (i.e. air gap /MUT/air gap) decreases. Similarly, for a non-zero fixed air layer thickness, as the MUT's relative permittivity increases the resonator's load formed by the three series capacitances decreases. Therefore, as the air gap widens the coupling between the sensor and the MUT is minimized. Consequently, a large air layer vanishes the coupling between the sensor and the loaded MUT a case at which the sensor's minimum transmission frequency becomes independent of the loaded MUT.

A case was considered and studied numerically to extract the relative permittivity of a loaded MUT at the presence of variable air gap layers using a 6-mm CSRR based sensor. The air gap layer in the considered case was varied from 0 mm to 100 um with a 10-um step. The relation of the change in the minimum transmission frequency magnitude and percentages ($\Delta f_{air\_gap}^{tmin}$), ($\Delta f_{air\_gap}^{tmin}\%$) are shown in (9) and 10), respectively. In these two relations, ($f_{MUT0}^{tmin}$) refers to minimum transmission frequency with a 0-mm air gap while ($f_{MUT1}^{tmin}$) refers to the minimum transmission frequency when an air gap exist between the CSRR and the loaded MUT. Fig.17 shows the change in the minimum transmission frequency with respect to the air gap thickness and the MUT's relative permittivity. The figure verifies the discussed air gap effect. The positive frequency shift percentages indicate that the change in the minimum transmission frequency moves toward the free space the change in the minimum transmission frequency as the air layer thickness and/or the MUT permittivity increase(s) which implicitly indicate that the coupling between the sensor and the loaded MUT decreases in either case.

$$\Delta f_{air\_gap}^{tmin} = f_{MUT1}^{tmin} - f_{MUT0}^{tmin} \tag{9}$$

$$\Delta f_{air\_gap}^{tmin}\% = \left(\frac{f_{MUT1}^{tmin} - f_{MUT0}^{tmin}}{f_{MUT0}^{tmin}}\right) \times 100 \tag{10}$$

## VII. Conclusion

This paper proposed relative permittivity sensors using MTL loaded with single scalable CSRR. In the beginning, the paper provided a smooth and sufficient theoretical background that rationalizes the selection of MTL as a resonator's host and CSRR as a sensor's resonating element. After that, the study discussed and verified through a systematic sensitivity analysis, the superiority of cross polarization excitation scheme over the frequently utilized pure electric excitation scheme, a single CSRR over double one and the utilization of a thin substrate MTL over a thicker one for sensitivity purposes. Moreover, the paper proposed a condition of sensitivity uniformity which is crucial for precise and consistent measurements over different bands of operation. The effect of the anticipated air gap effect was also studied based on the discussed model.

Future work should focus on the improvement of CSRR topology to have a higher interaction with the exciting fields, hence provide higher sensitivity when utilized with thin MTL substrate and cross polarization excitation. The proposed sensors can be used for a wide range of applications including microfluidics, nondestructive and biomedical sensors.

## Appendix

In this appendix a sensitivity uniformity condition is extracted using previously presented mathematical relations.

A necessary condition for uniform sensitivity is to have

$$\Delta f_1^{tmin}\% = \Delta f_2^{tmin}\% \tag{AI.1}$$

where $\Delta f_1^{tmin}\%$ and $\Delta f_2^{tmin}\%$ are the change in the minimum transmission frequencies of the first and second sensors with two different CSRR sizes, respectively.

Dividing both sides by 100 and using (3) and (5), (AI.1) can be rewritten as

$$\frac{\frac{1}{2\pi\sqrt{L_{CSRR1}(C_{CSRR1}+C_{MUT1})}} - \frac{1}{2\pi\sqrt{L_{CSRR1}C_{CSRR1})}}}{\frac{1}{2\pi\sqrt{L_{CSRR1}(C_{CSRR1}+C_{MUT1})}}} = \frac{\frac{1}{2\pi\sqrt{L_{CSRR2}(C_{CSRR2}+C_{MUT2})}} - \frac{1}{2\pi\sqrt{L_{CSRR2}C_{CSRR2})}}}{\frac{1}{2\pi\sqrt{L_{CSRR2}(C_{CSRR2}+C_{MUT2})}}} \tag{AI.2}$$

where $L_{CSRR1}$ and $L_{CSRR2}$ are the equivalent inductances of the first and second CSRR based sensors, $C_{CSRR1}$ and $C_{CSRR2}$ are the equivalent capacitances of the first and second CSRR based sensors, $C_{MUT1}$ and $C_{MUT2}$ are the equivalent capacitances of the loaded MUT of the first and second CSRR based sensors, respectively.

Multiplying numerator and denominator of both sides by $(2\pi)$, multiplying numerator and denominator of the left side by $\left(\sqrt{L_{CSRR1}}\right)$ and multiplying numerator and denominator of the right side by $\left(\sqrt{L_{CSRR2}}\right)$, (AI.2) can be simplified to

$$1 - \frac{\sqrt{(C_{CSRR1}+C_{MUT1})}}{\sqrt{(C_{CSRR1})}} = 1 - \frac{\sqrt{(C_{CSRR2}+C_{MUT2})}}{\sqrt{(C_{CSRR2})}} \tag{AI.3}$$

which is equivalent to

$$\sqrt{1+\frac{C_{MUT1}}{C_{CSRR1}}} = \sqrt{1+\frac{C_{MUT2}}{C_{CSRR2}}} \tag{AI.4}$$

From which the condition of uniform sensitivity for CSRR based permittivity sensors is

$$\frac{C_{MUT1}}{C_{CSRR1}} = \frac{C_{MUT2}}{C_{CSRR2}} \tag{AI.5}$$

Following a similar procedure, the condition of uniform sensitivity for CSRR based permeability sensors is

$$\frac{L_{MUT1}}{L_{CSRR1}} = \frac{L_{MUT2}}{L_{CSRR2}} \tag{AI.6}$$

(AI.5) and (AI.6) indicate that for a uniform sensitivity over different bands of frequency, if the CSRR is scaled to vary the operation frequency, a corresponding MUT's scaling by the same ratio shall also be implemented to vary its equivalent reactive element of interest (equivalent capacitance for a permittivity sensor and equivalent inductance for a permeability sensor).

In this paper, the width and length of the MUT that are interfaced with the CSRR footprint were identical and assumed to be two times higher than the side length of the square CSRR to meet the derived uniformity condition.

## ACKNOWLEDGMENT

The first author would like to thank the Saudi Arabian Oil Company (Saudi Aramco) for granting him a PhD degree scholarship.

## REFERENCES

[1] D. K. Ghodgaonkar, V. V. Varadan, and V. K. Varadan, "Free-space measurement of complex permittivity and complex permeability of magnetic materials at microwave frequencies," *IEEE Trans. Instrum. Meas.*, vol. 39, no. 2, pp. 387–394, Apr. 1990.

[2] W. E. Courtney, "Analysis and evaluation of a method of measuring the complex permittivity and permeability microwave insulators," *IEEE Trans. Microw. Theory Techn.*, vol. MTT-18, no. 8, pp. 476–485, Aug. 1970.

[3] J. Baker-Jarvis, E. J. Vanzura, and W. A. Kissick, "Improved technique for determining complex permittivity with the transmission/reflection method," *IEEE Trans. Microw. Theory Techn.*, vol. 38, no. 8, pp. 1096–1103, Aug. 1990.

[4] Y. Kobayashi and M. Katoh, "Microwave measurement of dielectric properties of low-loss materials by the dielectric rod resonator method," *IEEE Trans. Microw. Theory Techn.*, vol. TMTT-33, no. 7, pp. 586–592, Jul. 1985.

[5] N.-E. Belhadj-Tahar, A. Fourrier-Lamer, and H. de Chanterac, "Broadband simultaneous measurement of complex permittivity and permeability using a coaxial discontinuity," *IEEE Trans. Microw. Theory Techn.*, vol. 38, no. 1, pp. 1–7, Jan. 1990.

[6] D. K. Ghodgaonkar, V. V. Varadan, and V. K. Varadan, "A free-space method for measurement of dielectric constants and loss tangents at microwave frequencies," *IEEE Trans. Instrum. Meas.*, vol. 38, no. 3, pp. 789–793, Jun. 1989.

[7] P. A. Bernard and J. M. Gautray, "Measurement of dielectric constant using a microstrip ring resonator," *IEEE Trans. Microw. Theory Techn.*, vol. 39, no. 3, pp. 592–595, Mar. 1991.

[8] V. V. Varadan, R. Ro, and V. K. Varadan, "Measurement of the electromagnetic properties of chiral composite materials in the 8-40 GHz range," *Radio Sci.*, vol. 29, no. 1, pp. 9–22, 1994.

[9] D. V. Blackham and R. D. Pollard, "An improved technique for permittivity measurements using a coaxial probe," *IEEE Trans. Instrum. Meas.*, vol. 46, no. 5, pp. 1093–1099, Oct. 1997.

[10] A.-H. Boughriet, C. Legrand, and A. Chapoton, "Noniterative stable transmission/reflection method for low-loss material complex permittivity determination," *IEEE Trans. Microw. Theory Techn.*, vol. 45, no. 1, pp. 52–57, Jan. 1997.

[11] M. D. Janezic and J. A. Jargon, "Complex permittivity determination from propagation constant measurements," *IEEE Microw. Guided Wave Lett.*, vol. 9, no. 2, pp. 76–78, Feb. 1999.

[12] M. S. Boybay and O. M. Ramahi, "Material characterization using complementary split-ring resonators," *IEEE Trans. Instrum. Meas.*, vol. 61, no. 11, pp. 3039–3046, Nov. 2012.

[13] C.-S. Lee and C.-L. Yang, "Complementary split-ring resonators for measuring dielectric constants and loss tangents," *IEEE Microw. Wireless Compon. Lett.*, vol. 24, no. 8, pp. 563–565, Aug. 2014.

[14] C.-S. Lee and C.-L. Yang, "Single-compound complementary split-ring resonator for simultaneously measuring the permittivity and thickness of dual-layer dielectric materials," *IEEE Trans. Microw. Theory Techn.*, vol. 63, no. 6, pp. 2010–2023, Jun. 2015.

[15] M. A. H. Ansari, A. K. Jha, and M. J. Akhta, "Design and application of the CSRR-based planar sensor for noninvasive measurement of complex permittivity," *IEEE Sensors J.*, vol. 15, no. 12, pp. 7181–7189, Dec. 2015.

[16] A. Raj, A. K. Jha, M. A. H. Ansari, M. J. Akhtar, and S. Panda, "Metamaterial-inspired microwave sensor for measurement of complex permittivity of materials," *Microw. Opt. Technol. Lett.*, vol. 58, no. 11, pp. 2577–2581, 2016.

[17] A. Ebrahimi, J. Scott, and K. Ghorbani, "Differential sensors using microstrip lines loaded with two split-ring resonators," *IEEE Sensors J.*, vol. 18, no. 14, pp. 5786–5793, Jul. 2018.

[18] A. Ebrahimi, J. Scott, and K. Ghorbani, "Transmission lines terminated with LC resonators for differential permittivity sensing," *IEEE Microw. Wireless Compon. Lett.*, vol. 28, no. 12, pp. 1149–1151, Dec. 2018.

[19] J. Baker-Jarvis *et al.*, "Dielectric characterization of low-loss materials a comparison of techniques," *IEEE Trans. Dielectr. Electr. Insul.*, vol. 5, no. 4, pp. 571–577, Aug. 1998.

[20] M. Tabib-Azar, N. S. Shoemaker, and S. Harris, "Non-destructive characterization of materials by evanescent microwaves," *Meas. Sci. Technol.*, vol. 4, no. 5, p. 583, 1993.

[21] M. Tabib-Azar and P. S. Pathak, "Nondestructive superresolution imaging of defects and nonuniformities in metals, semiconductors, dielectrics, composites, and plants using evanescent microwaves," *Rev. Sci. Instrum.*, vol. 70, no. 6, pp. 2783–2792, 1999.

[22] W. Withayachumnankul, K. Jaruwongrungsee, A. Tuantranont, C. Fumeaux, and D. Abbott, "Metamaterial-based microfluidic sensor for dielectric characterization," *Sens. Actuators A, Phys.*, vol. 189, pp. 233–237, Jan. 2013.

[23] A. Ebrahimi, W. Withayachumnankul, S. Al-Sarawi, and D. Abbott, "High-sensitivity metamaterial-inspired sensor for microfluidic dielectric characterization," *IEEE Sensors J.*, vol. 14, no. 5, pp. 1345–1351, May 2014.

[24] L. Su, J. Mata-Contreras, P. Vélez, A. Fernández-Prieto, and F. Martín, "Analytical method to estimate the complex permittivity of oil samples," *Sensors*, vol. 18, no. 4, p. 984, 2018.

[25] P. Vélez, K. Grenier, J. Mata-Contreras, D. Dubuc, and F. Martín, "Highly-sensitive microwave sensors based on open complementary split ring resonators (OCSRRs) for dielectric characterization and solute concentration measurement in liquids," *IEEE Access*, vol. 6, pp. 48324–48338, 2018.

[26] P. Vélez, J. Muñoz-Enano, K. Grenier, J. Mata-Contreras, D. Dubu, and F. Martín, "Split ring resonator-based microwave fluidic sensors for electrolyte concentration measurements," *IEEE Sensors J.*, vol. 19, no. 7, pp. 2562–2569, Apr. 2019.

[27] J. Naqui, C. Jan, A. Karami-Horestani, C. Fumeaux, and F. Martín, "Angular displacement and velocity sensors based on coplanar waveguides (CPWs) loaded with s-shaped split ring resonators (S-SRR)," *Sensors*, vol. 15, no. 5, pp. 9628–9650, 2015.

[28] J. Naqui and F. Martín, "Transmission lines loaded with bisymmetric resonators and their application to angular displacement and velocity sensors," *IEEE Trans. Microw. Theory Techn.*, vol. 61, no. 12, pp. 4700–4713, Dec. 2013.

[29] A. K. Horestani, C. Fumeaux, S. F. Al-Sarawi, and D. Abbott, "Displacement sensor based on diamond-shaped tapered split ring resonator," *IEEE Sensors J.*, vol. 13, no. 4, pp. 1153–1160, Apr. 2013.

[30] A. K. Horestani, D. Abbott, and C. Fumeaux, "Rotation sensor based on horn-shaped split ring resonator," *IEEE Sensors J.*, vol. 13, no. 8, pp. 3014–3015, Aug. 2013.

[31] J. Naqui and F. Martín, "Angular displacement and velocity sensors based on electric-LC (ELC) loaded microstrip lines," *IEEE Sensors J.*, vol. 14, no. 4, pp. 939–940, Apr. 2014.

[32] A. M. Albishi, M. S. Boybay, and O. M. Ramahi, "Complementary split-ring resonator for crack detection in metallic surfaces," *IEEE Microw. Wireless Compon. Lett.*, vol. 22, no. 6, pp. 330–332, Jun. 2012.

[33] A. M. Albishi and O. M. Ramahi, "Microwaves-based high sensitivity sensors for crack detection in metallic materials," *IEEE Trans. Microw. Theory Techn.*, vol. 65, no. 5, pp. 1864–1872, May 2017.

[34] S. A. Al-Otaibi and M. M. Tentzeris, "Development of surface crack sensors using fractal geometries of complementary split ring resonators," in *Proc. ASNT Annu. Conf.*, 2017, pp. 9–15.
[35] S. A. Al-Otaibi and M. M. Tentzeris, "Metasurface based surface crack sensor using asymmetric complementary split ring resonator," in *Proc. 27th ASNT Res. Symp.*, 2018, pp. 12–19.
[36] M. Puentes, C. Weiß, M. Schüßler, and R. Jakoby, "Sensor array based on split ring resonators for analysis of organic tissues," in *IEEE MTT-S Int. Microw. Symp. Dig.*, Jun. 2011, pp. 1–4.
[37] F. Falcone, T. Lopetegi, J. D. Baena, R. Marques, F. Martin, and M. Sorolla, "Effective negative-$\varepsilon$ stopband microstrip lines based on complementary split ring resonators," *IEEE Microw. Wireless Compon. Lett.*, vol. 14, no. 6, pp. 280–282, Jun. 2004.
[38] D. Ahn, J.-S. Park, C.-S. Kim, J. Kim, Y. Qian, and T. Itoh, "A design of the low-pass filter using the novel microstrip defected ground structure," *IEEE Trans. Microw. Theory Techn.*, vol. 49, no. 1, pp. 86–93, Jan. 2001.
[39] D. M. Pozar, *Microwave Engineering*. New York, NY, USA: Wiley, 2009.
[40] I. Yaqoob *et al.*, "Internet of Things architecture: Recent advances, taxonomy, requirements, and open challenges," *IEEE Wireless Commun.*, vol. 24, no. 3, pp. 10–16, Jun. 2017.
[41] J. D. Baena *et al.*, "Equivalent-circuit models for split-ring resonators and complementary split-ring resonators coupled to planar transmission lines," *IEEE Trans. Microw. Theory Techn.*, vol. 53, no. 4, pp. 1451–1461, Apr. 2005.
[42] J. Bonache, M. Gil, I. Gil, J. Garcia-Garcia, and F. Martin, "On the electrical characteristics of complementary metamaterial resonators," *IEEE Microw. Wireless Compon. Lett.*, vol. 16, no. 10, pp. 543–545, Oct. 2006.
[43] J. Naqui, M. Duran-Sindreu, and F. Martin, "Modeling split-ring resonator (SRR) and complementary split-ring resonator (CSRR) loaded transmission lines exhibiting cross-polarization effects," *IEEE Antennas Wireless Propag. Lett.*, vol. 12, pp. 178–181, 2013.
[44] C.-L. Yang, C.-S. Le, K.-W. Chen, and K.-Z. Chen, "Noncontact measurement of complex permittivity and thickness by using planar resonators," *IEEE Trans. Microw. Theory Techn.*, vol. 64, no. 1, pp. 247–257, Jan. 2016.

**Salem A. Alotaibi** (S'19) received the B.Sc. and M.Sc. degrees in electrical engineering from King Fahd University of Petroleum and Minerals, Dhahran, Saudi Arabia, in 2008 and 2012, respectively. He is currently pursuing the Ph.D. degree with the School of Electrical and Computer Engineering, Georgia Institute of Technology, Atlanta, GA, USA.

He joined the Saudi Arabian Oil Company (Saudi Aramco) in 2008, where he served as an Electrical Engineer, a Group Leader, a Radiation Protection Officer and a Supervisor of Conventional NDT and Project Support Unit before his leave for Ph.D. He holds five NDT level III certificates in RT, UT, MT, PT, and VT methods. He is currently a member of Saudi Aramco NDT Standard Committee and the ATHENA Research Group. His research interests include computational electromagnetics and the design of microwave planar metamaterials for sensing applications.

**Yepu Cui** (S'18) received the B.S. degree in electrical engineering from the Harbin Institute of Technology, Harbin, China, in 2017. He is currently pursuing the Ph.D. degree with the School of Electrical and Computer Engineering, Georgia Institute of Technology, Atlanta, GA, USA.

He is a member of the ATHENA Research Group. His research interests include the design of novel origami-inspired reconfigurable antennas and microwave components using additive manufacturing processes, such as inkjet and 3D printing technologies.

**Manos M. Tentzeris** (F'10) received the Diploma *(magna cum laude)* degree in electrical and computer engineering from the National Technical University of Athens, Athens, Greece, and the M.S. and Ph.D. degrees in electrical engineering and computer science from the University of Michigan, Ann Arbor, MI, USA.

He is currently the Ken Byers Professor of flexible electronics with the School of Electrical and Computer Engineering, Georgia Institute of Technology, Atlanta, GA, USA, where he heads the ATHENA Research Group (20 researchers). He has served as the Head of the GTECE Electromagnetics Technical Interest Group, the Georgia Electronic Design Center Associate Director of RFID/Sensors research, the Georgia Institute of Technology NSF-Packaging Research Center Associate Director of RF Research, and the RF Alliance Leader. He has helped develop academic programs in 3-D/inkjet-printed RF electronics and modules, flexible electronics, origami and morphing electromagnetics, highly integrated/multilayer packaging for RF and wireless applications using ceramic and organic flexible materials, paper-based RFID's and sensors, wireless sensors and biosensors, wearable electronics, green electronics, energy harvesting and wireless power transfer, nanotechnology applications in RF, microwave MEMs, and SOP-integrated (UWB, multiband, mmW, and conformal) antennas. He has authored more than 650 articles in refereed journals and conference proceedings, five books, and 25 book chapters. He was a Visiting Professor with the Technical University of Munich, Munich, Germany, in 2002, GTRI-Ireland, Athlone, Ireland, in 2009, and LAAS-CNRS, Toulouse, France, in 2010.

Dr. Tentzeris is a member of the URSI-Commission D, the MTT-15 Committee, and the Technical Chamber of Greece, an Associate Member of EuMA, and a Fellow of the Electromagnetic Academy. He was a recipient/co-recipient of the 2019 Humboldt Research Award, the 2018 Intel IEEE ECTC 2018 Best Student Paper Award, the 2017 Georgia Institute of Technology Outstanding Achievement in Research Program Development Award, the 2016 Bell Labs Award Competition 3rd Prize, the 2015 IET Microwaves, Antennas, and Propagation Premium Award, the 2014 Georgia Institute of Technology ECE Distinguished Faculty Achievement Award, the 2014 IEEE RFID-TA Best Student Paper Award, the 2013 IET Microwaves, Antennas and Propagation Premium Award, the 2012 FiDiPro Award in Finland, the iCMG Architecture Award of Excellence, the 2010 IEEE Antennas and Propagation Society Piergiorgio L. E. Uslenghi Letters Prize Paper Award, the 2011 International Workshop on Structural Health Monitoring Best Student Paper Award, the 2010 Georgia Institute of Technology Senior Faculty Outstanding Undergraduate Research Mentor Award, the 2009 IEEE TRANSACTIONS ON COMPONENTS AND PACKAGING TECHNOLOGIES Best Paper Award, the 2009 E. T. S. Walton Award from the Irish Science Foundation, the 2007 IEEE AP-S Symposium Best Student Paper Award, the 2007 IEEE MTT-S IMS Third Best Student Paper Award, the 2007 ISAP 2007 Poster Presentation Award, the 2006 IEEE MTT-S Outstanding Young Engineer Award, the 2006 Asia–Pacific Microwave Conference Award, the 2004 IEEE TRANSACTIONS ON ADVANCED PACKAGING COMMENDABLE Paper Award, the 2003 NASA Godfrey Art Anzic Collaborative Distinguished Publication Award, the 2003 IBC International Educator of the Year Award, the 2003 IEEE CPMT Outstanding Young Engineer Award, the 2002 International Conference on Microwave and Millimeter-Wave Technology Best Paper Award, Beijing, China, the 2002 Georgia Institute of Technology–ECE Outstanding Junior Faculty Award, the 2001 ACES Conference Best Paper Award, the 2000 NSF CAREER Award, and the 1997 Best Paper Award of the International Hybrid Microelectronics and Packaging Society. He was the Co-Chair of the 2019 IEEE APS Conference, the TPC Chair of the IEEE MTT-S IMS 2008 Symposium, and the Chair of the 2005 IEEE CEM-TD Workshop. He is the Vice-Chair of the RF Technical Committee (TC16) of the IEEE CPMT Society. He is the Founder and the Chair of the RFID Technical Committee (TC24) of the IEEE MTT-S and the Secretary/Treasurer of the IEEE C-RFID. He is an Associate Editor of the IEEE TRANSACTIONS ON MICROWAVE THEORY AND TECHNIQUES, the IEEE TRANSACTIONS ON ADVANCED PACKAGING, and the *International Journal on Antennas and Propagation*. He has given more than 100 invited talks to various universities and companies all over the world. He served as one of the IEEE MTT-S Distinguished Microwave Lecturers from 2010 to 2012 and one of the IEEE CRFID Distinguished Lecturers.